Available online at www.sciencedirect.com

SciVerse ScienceDirect

Solar Energy 86 (2012) 1552–1562

SOLAR ENERGY

www.elsevier.com/locate/solener

Simulated and experimental performance of a heat pipe assisted solar wall

Michael V. Albanese, Brian S. Robinson, Ellen G. Brehob, M. Keith Sharp *

Renewable Energy Applications Laboratory, Department of Mechanical Engineering, University of Louisville, 200 Sackett Hall, Louisville, KY 40292, United States

Received 2 July 2010; received in revised form 19 October 2011; accepted 18 February 2012
Available online 14 March 2012

Communicated by: Associate Editor Yogi Goswami

Abstract

Performance was evaluated for a passive solar space heating system utilizing heat pipes to transfer heat through an insulated wall from an absorber outside the building to a storage tank inside the building. The one-directional, thermal diode heat transfer effect of heat pipes make them ideal for passive solar applications. Gains by the heat pipe are not lost during cloud cover or periods of low irradiation. Simplified thermal resistance-based computer models were constructed to simulate the performance of direct gain, indirect gain, and integrated heat pipe passive solar systems in four different climates. The heat pipe system provided significantly higher solar fractions than the other passive options in all climates, but was particularly advantageous in cold and cloudy climates. Parametric sensitivity was evaluated for material and design features related to the collector cover, absorber plate, heat pipe, and water storage tank to determine a combination providing good thermal performance with diminishing returns for incremental parametric improvements. Important parameters included a high transmittance glazing, a high performance absorber surface and large thermal storage capacity.

An experimental model of the heat pipe passive solar wall was also tested in a laboratory setting. Experimental variations included fluid fill levels, addition of insulation on the adiabatic section of the heat pipe, and fins on the outside of the condenser section. Filling the heat pipe to 120% of the volume of the evaporator section and insulating the adiabatic section achieved a system efficiency of 85%. Addition of fins on the condenser of the heat pipe did not significantly enhance overall performance.

The computer model was validated by simulating the laboratory experiments and comparing experimental and simulated data. Temperatures across the system were matched by adjusting the model conductances, which resulted in good agreement with the experiment.

Keywords: Solar; Passive; Heat pipe; Water wall; Solar fraction; Isolated gain

1. Introduction

To meet the Intergovernmental Panel on Climate Change (IPCC) target to limit global temperature rise to 2 °C, developed countries must reduce carbon emissions by 80% below 1990 levels by 2050, which will require drastic changes by all energy users. Buildings account for 40% of total US energy use, which comprises 72% of all electrical energy and 55% of natural gas, and release 39% of total US carbon dioxide emissions (URL 1, 2010). This impact is not only the largest among all sectors, but is also perhaps the easiest to reduce by substantial amounts. Passive solar systems are particularly suited to space heating, which accounts for 31% of typical home energy use alone (URL 2, 2010). Conventional direct gain and indirect gain passive solar systems typically contribute net gains of energy during sunny weather

* Corresponding author. Address: Department of Mechanical Engineering, University of Louisville, Louisville, KY 40292, United States. Tel.: +1 502 852 7280 (Office); fax: +1 502 852 6053.
E-mail address: keith.sharp@louisville.edu (M. Keith Sharp).

0038-092X/$ - see front matter © 2012 Elsevier Ltd. All rights reserved.
doi:10.1016/j.solener.2012.02.017

Nomenclature

Variables

A	area
A_i	anisotropy index
$f_d = (I_d/I)^{0.5}$	beam fraction of total insolation
I	hourly total insolation, without subscript on horizontal surface
K	network conductance
M	product of mass and specific heat
R	ratio of radiation on tilted surface to horizontal surface
S	solar gain
t	time
T	temperature

Greek symbols

β	collector tilt
η	efficiency
ρ	reflectance
$(\tau\alpha)$	transmittance–absorptance product

Subscripts

b	beam radiation
c	collector
d	diffuse radiation
g	ground reflected radiation
i,j	thermal node numbers
0	previous time step

conditions, but suffer losses greater than a nonsolar insulated wall during nighttime and cloudy periods. Traditional thermosyphoning isolated gain systems need not have increased losses, but typically require solar collectors below the heated space (Fig. 1).

The proposed heat pipe system incorporates a heat pipe to transfer heat through an insulated wall from the solar absorber to the thermal mass (Fig. 2). Heat pipes transfer heat in only one direction, similar to thermosyphons, but use a two-phase fluid that provides improved heat transfer and requires little elevation difference between the evaporator and condenser sections. Liquid is boiled in the lower evaporator section of the heat pipe and the vapor rises to the upper condenser end, where the vapor condenses and transfers its energy (Fig. 3). The condensate then falls by gravity back to the evaporator.

Passive solar space heating utilizing heat pipes was initially investigated by Corliss (1979), who developed a computer simulation to analyze passive solar heating for a variety of climates. The heat pipe system performed better in all climates. Corliss also built a prototype constructed by epoxying heat pipes into groves in the absorber plates with the condensers placed into plastic water tanks. The absorber plates were painted black and the heat pipes were filled with dichlorofluoromethane (Freon-21) and placed at a 5° angle to allow gravity to return the condensate to the evaporator section. *R*-20 insulation was placed between the absorber plate and the water wall. Corliss also completed an economic and marketability assessment of the heat pipe system. Large load to collector area ratio installations in new homes offered the highest cost effectiveness.

A review of several passive solar heating systems incorporating heat pipes is found in the paper by Rice (1984). The author examined actual building performance and simulated data to conclude that simplicity and performance made these systems worth additional investigation. van Dijk et al. (1984), built a passive solar space heater using heat

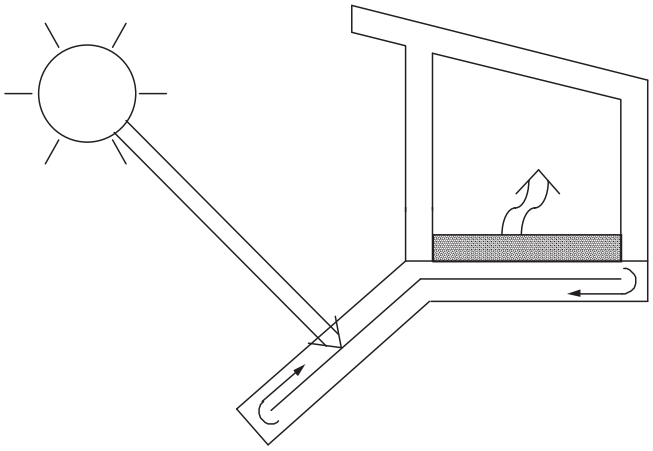

Fig. 1. Isolated gain passive solar system with thermosyphoning collector.

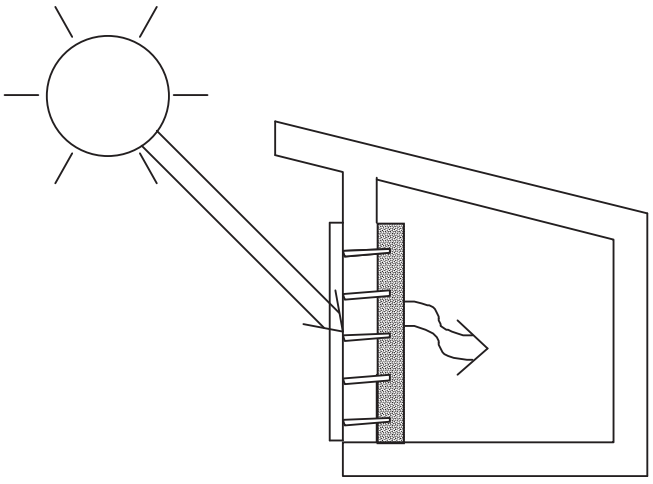

Fig. 2. Isolated gain system with integrated heat pipes, which provide one-way heat transfer from the outdoor absorber to the indoor thermal mass.

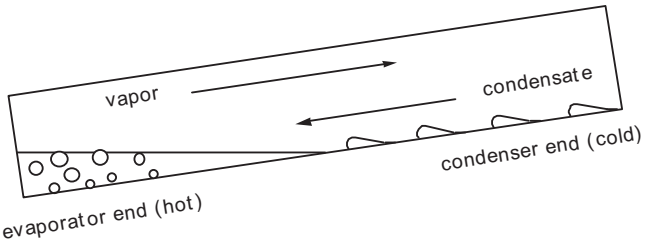

Fig. 3. Heat pipe operation. When the lower evaporator end is hotter than the higher condenser end, heated vapor rises and condensate falls. When the evaporator end is colder than the condenser, this two-phase heat transfer cycle ceases.

pipes to achieve higher efficiencies than traditional concrete wall systems. This system separated the living space from the condenser section of the heat pipes by placing insulation between the two areas. This created an air cavity that would be heated during insolation periods. Vents at the top and the bottom of the air cavity allowed convection to disperse the heat throughout the room. This design was tested in laboratory settings and in real climate conditions. This heat pipe design significantly reduced the overall weight of the space heater and achieved higher gains than traditional concrete Trombe walls. The cost benefit ratio was competitive compared to active solar space heaters. Saman and Abdulla (1983) and Varga et al. (2002) used heat pipes to transfer heat away from a building by placing the evaporator sections of heat pipes in the building's wall structure and on the inside wall, respectively. The condensers were exposed to ambient conditions. Saatci and Olwi (1989) tested the potential for downward heat transfer in heat pipes by using capillary action to return liquid to the evaporator.

Analysis of a heat pipe passive solar system was conducted by Susheela and Sharp (2001). Computer simulations were performed comparing a heat pipe system to water and concrete Trombe walls in three climates. Again analysis showed that the heat pipe system performs better in all climates, and especially well in cold and cloudy climates. A prototype tested in Salt Lake City, UT, demonstrated collector efficiencies were 40–60% during peak solar periods, and heat pipe efficiencies of 60–80%. Susheela and Sharp recommended that an insulated heat pipe adiabatic section, optimized fill fraction of the heat transfer fluid, and condenser fins might improve system performance.

In the current study, (i) a computer model was developed to further investigate the feasibility of heat pipe integrated walls in a range of climates, (ii) a parametric study was conducted to determine the design features that have a significant effect on performance, and (iii) a prototype heat pipe wall was constructed and tested in a laboratory setting to provide validation data.

2. Methods

2.1. Computer models

MatLab codes were created to simulate hourly performance of the heat pipe system, as well as direct gain and concrete and water wall indirect gain systems. The thermal network approach (Fig. 4 and Table 1) was adapted from Susheela and Sharp (2001), who used a modified version of algorithms developed by Corliss (1979). Parametric sensitivity was evaluated in ranges around these baseline values.

For each node in the thermal network, the energy balance equation was

$$M_i\left(\frac{dT_i}{dt}\right)=\sum_j(K_{ij}(T_j-T_i)+S_i) \tag{1}$$

Using a center difference discretization scheme, Eq. (1) becomes

$$\left(\frac{2M_i}{\Delta t}+\sum_j K_{ij}\right)T_i-\sum_j K_{ij}T_j = \frac{2M_iT_{i0}}{\Delta t}+\sum_j K_{ij}(T_{j0}-T_{i0})+S_i+S_0 \tag{2}$$

A set of Eq. (2) for all nodes was simultaneously solved for nodal temperatures as a function of time, beginning with a set of initial temperatures. Iterations were used to calculate heat transfer coefficients dependent on nodal temperatures. Room nodal temperatures were restricted to simulate auxiliary heating and venting, keeping room temperatures at 19–24 °C. Typical Meteorological Year Data (TMY3) provided hourly ambient temperatures and radiation levels.

Four cities were chosen to provide a range of insolation and temperatures (Fig. 5). Albuquerque, NM, and Rock Springs, WY, receive significantly more solar radiation than Louisville, KY, and Madison, WI. On the other hand, Rock Springs and Madison are considerably colder than Albuquerque and Louisville.

Absorbed solar radiation S – An anisotropic model was used that includes three components of diffuse radiation – uniform, circumsolar, and horizon brightening (Hay and Davies, 1980; Klucher, 1979; Reindl et al., 1990)

$$S=(I_b+I_dA_i)R_b(\tau\alpha)_b+I_d(1-A_i) \times(\tau\alpha)_d\left(\frac{1+\cos\beta}{2}\right)\left(1+f_d\sin^3\left(\frac{\beta}{2}\right)\right) +I\rho_g(\tau\alpha)_g\left(\frac{1-\cos\beta}{2}\right) \tag{3}$$

2.1.1. Heat Pipe System Model

The heat transfer modes included for each network conductance value are summarized below. More detail can be found in (Albanese, 2009 and Susheela and Sharp, 2001).

Overall collector heat transfer coefficient K_{71} – The overall loss coefficient from the absorber was the sum of the top and edge losses (Duffie and Beckman, 2006). Bottom losses were treated separately as additional heat to the system since when the absorber is hot, heat transfers through the insulation into the storage tank. Convective losses to

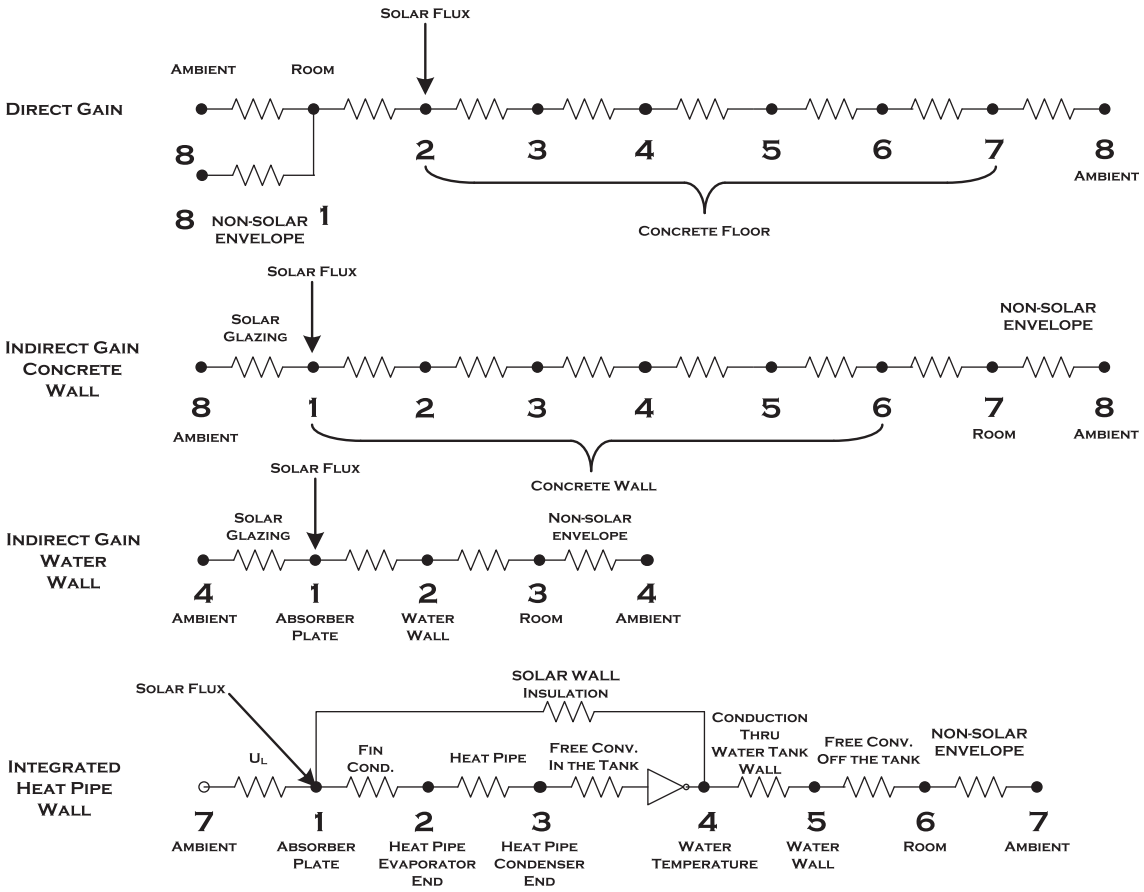

Fig. 4. Thermal networks for passive solar computer simulations.

Table 1
Baseline conductance values.

	K_{81g}	K_{81b}	K_{12}	K_{23}	K_{34}	K_{45}	K_{56}	K_{67}	K_{78}	K_{41}	K_{71}	$K_{81b} + K_{78}$ total room-ambient
Direct Gain	2.83	7.63	5.67	26.7	13.1	13.1	13.1	26.7	2.37	–	–	10
Concrete Wall	2.83	–	26.7	13.1	13.1	13.1	26.7	5.67	10	–	–	–
Water Wall	–	–	56.7	5.67	10	–	–	–	–	2.83	–	–
Heat Pipe Wall	–	–	115.1	[1]	[2]	385.2	[2]	10	–	0.648	[2]	–

[1]: $K_{23} = 12.034$ W/m^2 K $T_1 > T_4$, $= 0.0$ W/m^2 K for $T_1 < T_4$.
[2]: Temperature dependent conductance.
All conductance values are normalized by collector area.

ambient were calculated with wind speed obtained from the TMY3 data.

Absorber plate fin conduction K_{12} – The heat transfer coefficient between the absorber plate and the evaporator end of the heat pipe was derived from the conduction of the fin to the heat pipe (Susheela and Sharp, 2001).

Heat pipe conductance K_{23} – The conductance through the heat pipe includes conduction through the pipe wall of the evaporator, boiling heat transfer to the fluid, convection of vapor up the heat pipe, condensing heat transfer to the wall of the condenser section and conduction through the wall (Incropera and DeWitt, 2002). The conductance due to the phase change was assumed to be so large compared to the conductance through the walls that it could be neglected.

Tank free convection K_{34} – The natural convection from the condenser section of the heat pipe to the water in the tank was calculated (Incropera and DeWitt, 2002).

Tank wall conduction K_{45} – Conductive transport through the wall of the storage tank was included.

Room air free convection K_{56} – The conductance between the wall of the tank and the room air was found for the free convection of air around each face of the tank (Incropera and DeWitt, 2002).

Non-solar building envelope losses K_{67} – This conductance included the UA values of all nonsolar building elements, as well as ventilation losses, normalized by the collector area.

Solar wall insulation K_{41} – When the temperature at (node 4), the water temperature in the thermal storage

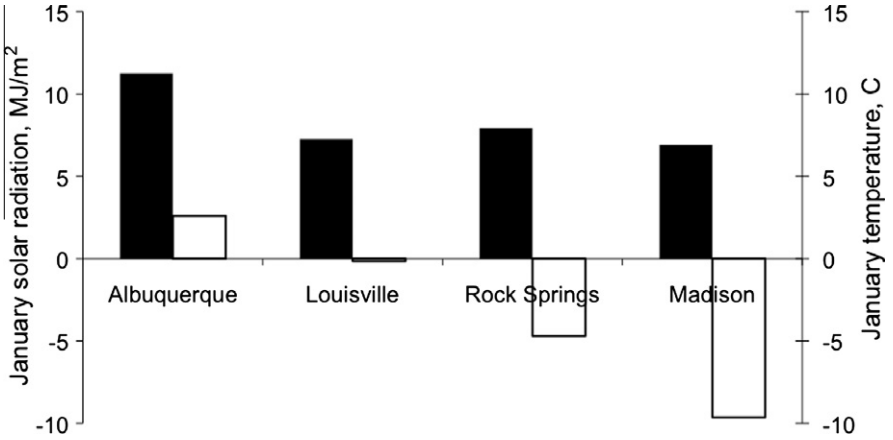

Fig. 5. Average daily radiation (dark bars) and ambient temperature (light bars) for January [TMY3].

tank, is greater than node 2 (the evaporator end of the heat pipe), the condensate remains in the evaporator and essentially no heat is transferred through the heat pipe. Under these circumstances, heat is transferred primarily through the wall insulation from the tank to the absorber plate. The heat transfer between nodes 4 and 1 in this case represents the heat losses during cloud cover and nighttime conditions. Conduction along the walls of the heat pipes was neglected. The solar wall conductance value was calculated using thermal conductivity and thickness for each building material in the wall. The insulation between the water tank and absorber plate provides a large thermal resistance and makes the overall conductance relatively small.

The influence of design variables for a heat pipe passive solar wall were individually simulated. Results were compared based on the solar fraction, defined as the percentage of the space heating load supplied by the passive solar system. The baseline values of the variables that were investigated are listed in Table 2.

Table 2
Heat pipe system base case parameters.

City	Louisville, Kentucky
Cover (number)	1
Cover (thickness)	0.003175 (m)
Cover (emittance)	0.88
Cover (extinction coefficient)	4 (m^{-1})
Absorber plate (material)	Copper
Absorber plate (selective surface)	Black chrome
Absorber plate (thickness)	0.003175 (m)
Absorber plate (insulation thickness)	0.025 (m)
Absorber plate (insulation conductivity)	0.05 (W/m K)
Absorber plate (height)	2.083 (m)
Absorber plate (width)	1.1652 (m)
Heat pipe (number, spacing)	5, 0.3471 (m)
Heat pipe (material)	Copper
Heat pipe (inclination angle)	(No vapor column conductance)
Heat pipe (wick structure)	(None)
Condenser fin (number)	(None)
Water tank (number)	1
Water tank (height)	1.9558 (m)
Water tank (length)	1.1906 (m)
Water tank (width)	0.2032 (m)
Water tank (wall thickness)	0.003175 (m)
Water tank (material conductivity)	0.5 (W/m K)
Solar wall insulation conductance	0.648 (W/m^2 K)
Ground reflectance	0.3
Load to collector area ratio	10 (W/m^2 K)

2.1.2. Direct gain and concrete and water wall indirect gain models

Derivations of the conductances for the direct gain and indirect gain systems are for the sake of brevity not shown, but are given in Table 1.

2.2. Experimental methods

2.2.1. Experimental apparatus

The experimental model (Fig. 6) was built using one heat pipe attached to a black chrome plated copper absorber plate. An aluminum frame was constructed to hold a low-iron glass cover and both the frame and the absorber plate were attached to an insulating wall at an angle of 4.5°. Behind the insulating wall, 189.3 L (50 gallons) of water in a plastic tank served as a thermal storage device. The tank was insulated to *R*-20.

Two condensers sections were fabricated for testing, one a smooth 0.0254 m (1 in.) diameter copper pipe and the other an identical pipe with 0.003175 m (1/8 in.) thick copper fins with 0.03175 m (1–1/4 in.) O.D. 180 fins were soldered on every 0.00635 m (1/4 in.). The condenser section was inserted into the tank via a bulkhead fitting.

Three 1000 W metal halide bulbs spaced 0.514 m (20–1/4 in.) apart were used to simulate solar radiation. To create uniform radiation across the absorber plate, reflectors were built of aluminum foil and insulation board and the lamps were fitted with aluminum foil blinders 0.076 m (3 in.) in width. The lamps were placed 1.143 m (45 in.) from the absorber plate.

The heat pipe was charged with DuPont SUVA-124, a retrofit HCFC refrigerant for applications originally designed for *R*-114 and *R*-124. The heat pipe was first

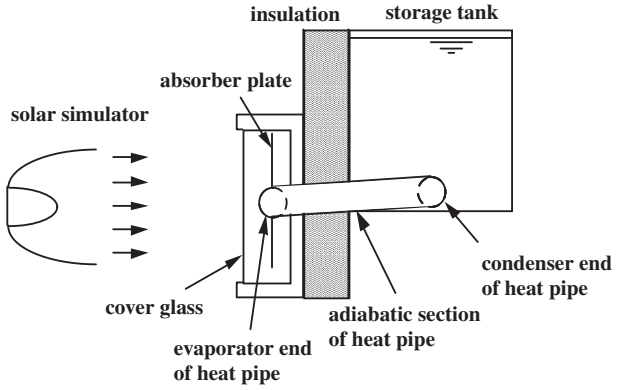

Fig. 6. Diagram of experimental apparatus.

washed and then evacuated to 723.9 mm (28.5 in.) of mercury vacuum. During filling, the refrigerant tank was weighed to determine the amount of working fluid used. The charging volume was based on percentages of evaporator volume.

2.2.2. Instrumentation

28 T-type thermocouples were used to measure temperatures, eight on the absorber, four on the evaporator section, four on the condenser section, three on the adiabatic section, eight in the water tank and one for ambient air. Four Kipp and Zonen CM3 pyranometers were placed near the corners of the collector frame to measure radiation.

A National Instruments SCXI chassis was used in conjunction with the SCXI-1600, 16 bit digitizer module, and the SCXI-1102/B/C module. The SCXI-1102/B/C module is used for signal conditioning of thermocouples, and low-bandwidth volt and millivolt sources. LabVIEW programs were written for all data acquisition.

2.2.3. Error propagation

The pyranometers had an overall error of ±2% or ±18.4 W/m^2. The thermocouples had an error of ±0.1 K. Errors associated with digitization, system noise, offset, and temperature drift for the SCXI 1600 and SCXI 1102 amounted to ±2.4 mV or ±0.25 K. The resulting overall uncertainty of temperature measurements was ±0.27 K, or about 0.1% for temperatures around 300 K. For errors in water volume of ±1% and time of ±0.001%, the root sum squared error of system efficiency was estimated to be ±2.24%.

2.2.4. Experimental protocol

The heat pipe system model was tested with both an insulated and un-insulated adiabatic section. A range of fluid fill levels was also tested using a smooth un-finned condenser section. The finned condenser was then tested using only the optimum fill level.

Each test began with the lamps turned on and warmed up, and with a tank temperature below 23 °C. Data collection was started once the water tank temperature had reached 23 °C and continued to 26.5 °C. The rate of heat addition to the tank of water was determined by its rate of temperature rise and using known values for the mass and specific heat of water. Conservative estimates of overall system efficiency were calculated by neglecting thermal losses from the tank

$$\eta = \frac{M\frac{\Delta T_s}{\Delta t}}{SA_c} \tag{4}$$

Each case was run three times to evaluate repeatability.

2.3. Matching of experiment and simulation

To better understand the performance of the heat pipe in the experiments, and to provide partial validation of the computer simulation, a simulation was run with inputs and parameter values mimicking those of the experiments with 120% fill and insulated adiabatic section. Initial changes to parameter values included absorber plate area (2.43 m^2), number of heat pipes (one) and mass specific heat product of the water (816,920 J/m^2 K). To model the insulation around the tank, conductance of the tank wall, K_{45}, was decreased by a factor of 10^9, which simplified the model, making the results insensitive to conductances K_{56} and K_{67}. Note that the heat pipe added heat to the tank continuously throughout the experiments, therefore, the matching simulations were also insensitive to K_{41}. Inputs from experimental data were initial tank temperature, input radiation and ambient temperature. All nodes in the simulation had zero mass except the water tank, therefore, these simulated nodal temperatures increased immediately compared to the experiments. For this reason, temperatures were compared only after startup transients had asymptoted to the quasi-steady increase of system temperatures. After this initial comparison, heat pipe conductance K_{23} was manually adjusted to better match the experimental temperatures.

3. Results

3.1. Simulations

3.1.1. Example nodal temperatures

The nodal temperatures and solar radiation for the baseline heat pipe system (Table 2) during a 1-week period in late January for Louisville, KY are shown in Fig. 7. The absorber plate experienced the highest temperatures throughout sunny days. The evaporator section was slightly cooler during these times, representing the fin efficiency of the absorber, and the condenser section followed nearly the same temperature as the evaporator. When the sun went down, the absorber and evaporator cooled to near ambient temperature. The thermal diode effect of the system is evident in low evening temperature drops experienced by the condenser and water tank. Gains to the room were evident during consecutive days of high radiation and warmer than

average ambient temperatures. The levels of radiation show that for this time period there were both cloudy and sunny days.

3.1.2. Comparison of heat pipe system performance to direct and indirect gain

The direct gain system performed better than the concrete wall in Albuquerque, which was the warmest and clearest of the four climates (Fig. 8). Direct gain produced a small net loss in the cold, cloudy climate of Madison. The concrete wall system provided more heat than the direct gain system in all climates except Albuquerque. The water wall system outperformed the concrete wall in all climates. The heat pipe system outperformed all other passive solar systems in all climates.

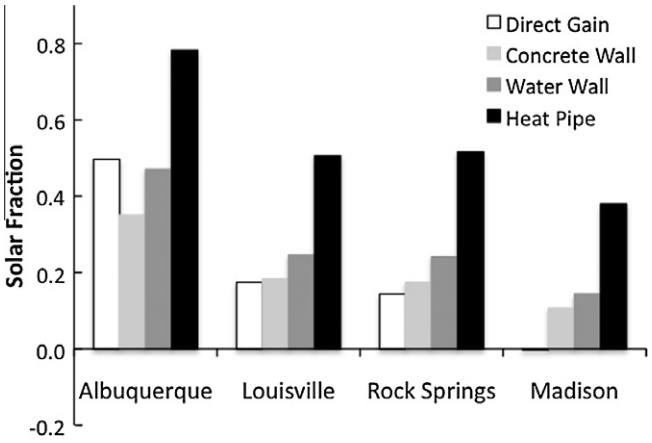

Fig. 8. Climate comparison of passive solar systems.

3.1.3. Parametric sensitivity

Load to collector ratio – Increasing K_{67} decreased the solar fraction (Fig. 9). A load to collector ratio of 10 W/m^2 K was chosen for the baseline case and resulted in a solar fraction of 50.60% in Louisville.

Absorber covers – Two covers improved the solar fraction by only 0.4%, from 50.60% to 50.81%.

Thickness of cover glass – Increasing the glass thickness from 1/8 to 1/4 in. decreased the solar fraction by 2.4%.

Glass extinction coefficient – System performance was improved by 8.2% by using low iron glass with extinction coefficient of 4 m^{-1} compared to 32 m^{-1} for common high iron window glass.

Absorber surface – Bare copper and aluminum have low absorptivity and emissivity, and yielded low system performance (Fig. 10). (On Figs. 10 and 11, the baseline parameter value is marked with an asterisk.). Black painted absorbers have high absorptivity and emissivity, and improved performance significantly. However selective surfaces with high solar absorptivity and low thermal emissivity provided greater performance. Black chrome (absorptivity of 0.96 and emissivity of 0.02) is commonly used in the solar industry and yielded a 22.9% increase in solar fraction compared to a flat black paint finish. Black copper and black nickel electroplating is not as common, is more expensive to apply, and had similar performance. The higher thermal conductivity of a copper absorber plate improved performance a small amount relative to aluminum.

Absorber thickness – An increase in absorber plate thickness from 1/8 in. to 1/4 in. increased performance by only 0.6%.

Collector edge insulation – Doubling the thickness from the base case of 0.025 m caused a less than 0.1% improvement in solar fraction.

Heat pipe material – Switching the copper heat pipes to aluminum reduced the solar fraction by less than 0.6%.

Number of heat pipes – Changing from five heat pipes to four decreased the solar fraction by less than 0.4%. (Note that the spacing of the heat pipe decreases as more heat pipes are added, while the height of the heat pipe wall

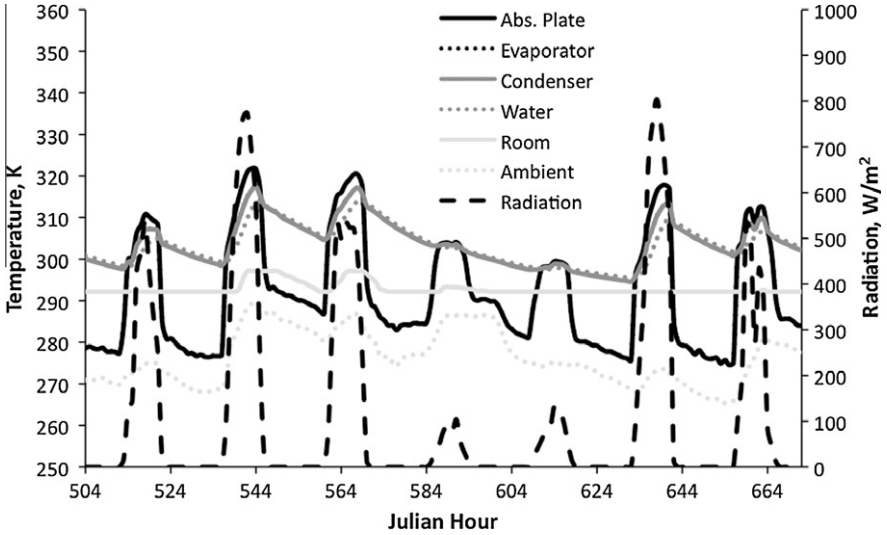

Fig. 7. Simulated solar radiation and resulting nodal temperatures.

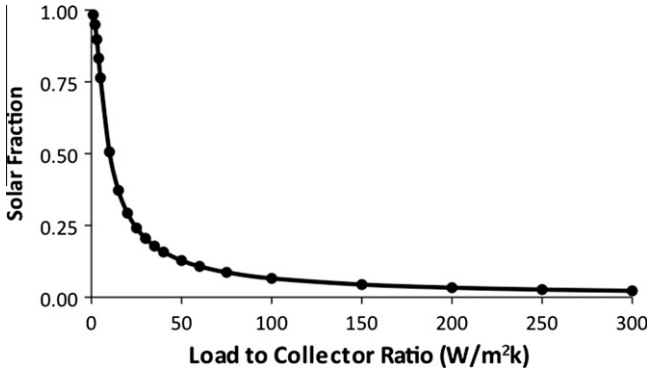

Fig. 9. Effect of load to collector ratio on system performance.

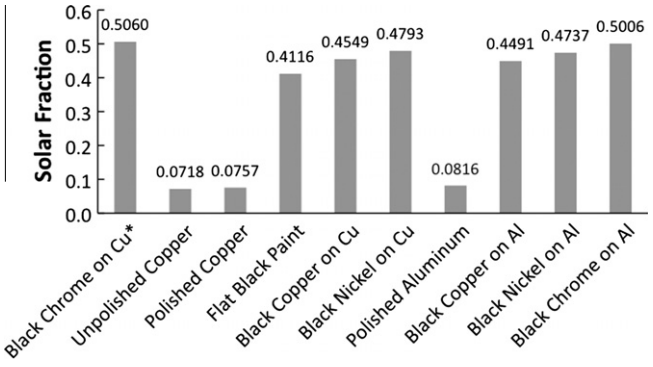

Fig. 10. Effect of absorber plate material and selective surfaces on system performance.

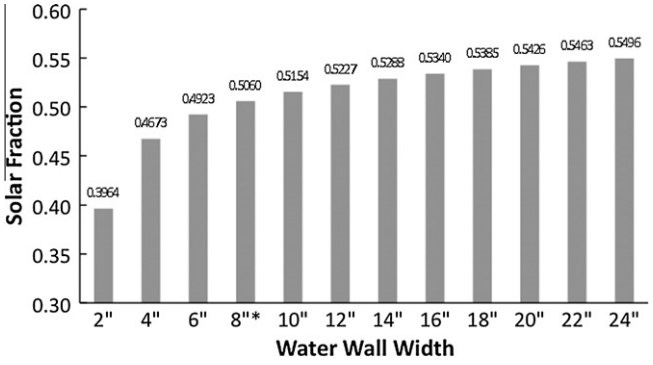

Fig. 11. Effect of water wall width on system performance.

remained the same for all cases.) Doubling the number of heat pipes increased the performance by about 0.5%.

Thermal storage capacity – Decreasing thermal storage capacity by reducing the water tank width by one half from the baseline reduced the solar fraction by 7.6% (Fig 11). A 75% reduction cut the solar fraction by 21.7%. Doubling the water tank volume increased the solar fraction by 5.5%.

Tank outer convection coefficient – Specific tank designs were not analyzed, however, decreasing the convection coefficient by 20% decreased the solar fraction by about 0.8%. Increasing the convection coefficient by 20% increased the solar fraction by about 0.5%.

Tank wall conductivity and thickness – Conductivity over the range of 0.2–0.8 W/m K changed the solar fraction by less than 0.15%. Increasing the thickness of a baseline tank wall (plastic with thermal conductivity of 0.5 W/m K) from 1/8 in. to 3/8 in. reduced the solar fraction by only 0.14%.

Heat pipe condenser fins – The addition of 91 fins with thickness of 0.125" and outside diameter of 1.25" increased the solar fraction by 0.2%. Increasing the number of fins to 366 increased the solar fraction by 0.5%. Using 91 fins with thickness of 0.125" for all cases, increasing fin diameter to 2" increased performance by 0.6% compared to no fins. Increasing the thickness of 91 fins of 1.25" diameter to 0.5" increased solar fraction by 0.6%.

Wall insulation – Decreasing the conductivity of the insulation between the water tank and absorber plate by 20% increased the solar fraction by 0.6%, while increasing it by 20% decreased the solar fraction by 0.5%.

3.2. Experimental results

3.2.1. Radiation distribution

The average radiation value measured among the fifteen locations across the absorber plate was 709.4 W/m^2. The maximum and minimum values were 757.3 W/m^2 and 645.8 W/m^2, respectively. The distribution was higher in the center and lower around the edges. The final orientation for the solar lamps achieved a standard deviation of 4.46% of the mean, and the maximum percentage difference across the absorber plate was 14.7%. TMY3 data for Louisville shows maximum radiation on a vertical surface during winter periods up to about 811 W/m^2, thus the radiative power provided by the lamps was in the range of a moderately sunny day in this climate.

3.2.2. Fill level and adiabatic insulation

An example set of three runs for an un-insulated adiabatic section and 80% fill volume is shown in Fig. 12. The average rate of temperature change was 1.136 °C/h, with standard deviation of 1.1% of the mean. Radiation was 700.45 W/m^2 ± 1.52%. The variation in radiation among runs within a set was similarly small for all cases.

A fill level of 120% of the volume of the evaporator section provided the greatest heating rate for both the insulated and uninsulated adiabatic section (Table 3). Adding condenser fins for the 120% fill level increased the heating rate by less than 0.2%. The 120% fill level provided statistically significant improvements over the 100% and 140% fill levels with 99% and 92% confidence, respectively (Table 4). There was no significant performance difference between finned and smooth condensers ($p = 0.943$).

3.2.3. Overall system efficiency

Insulating the adiabatic section of the heat pipe improved overall system efficiency for all fill levels, and a 120% charging level produced the highest efficiency (Fig. 13).

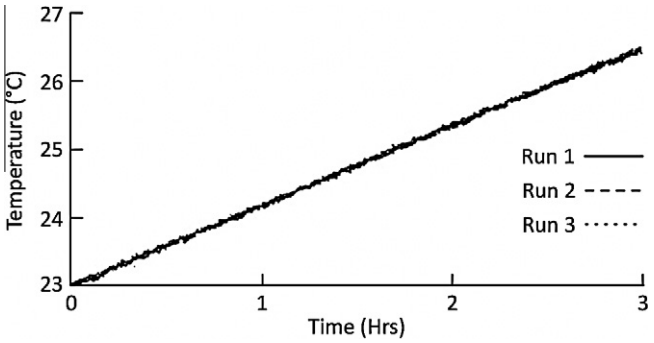

Fig. 12. Water tank temperature (uninsulated adiabatic section/80% fill).

Table 3
Water tank heating rates for varying charge levels and insulation on the adiabatic section.

Fill level	Uninsulated		Insulated	
	Ave. temperature change (°C/h)	Std. deviation/ mean (%)	Ave. temperature change	Std. deviation/ mean (%)
80%	1.136	1.1	1.153	0.6
100%	1.160	1.9	1.195	1.0
120%	1.190	1.1	1.227	1.1
140%	1.176	0.5	1.203	1.8
120% with finned condenser	–	–	1.229	1.4

Table 4
P-values for pairwise comparison of fluid fill levels.

	80%	100%	120%
100%	0.0025		
120%	0.0000	0.0051	
140%	0.0002	0.53	0.076

3.3. Matching of experiment and simulation

Fig. 14 shows the experimental and simulated water tank temperatures after matching. K_{71} and K_{34} were not adjusted, but were temperature dependent (Table 5). Recall that K_{45} was set to a billionth of its modeled value to simulate the high level of insulation around the water tank used in the experiment. Only the heat pipe conductance K_{23} was adjusted to achieve the fit in Fig. 14.

4. Discussion

4.1. Simulations

The heat pipe system provided significantly higher performance than direct and indirect gain passive solar systems in all four climates tested. The thermal diode effect of the heat pipes allows effective transfer of heat into storage and low losses in the opposite direction. Losses can be reduced in conventional direct and indirect gain systems by adding nighttime insulation, however, high *R*-values can be inconvenient to achieve, manual or automatic control is required, and appearance can be an issue.

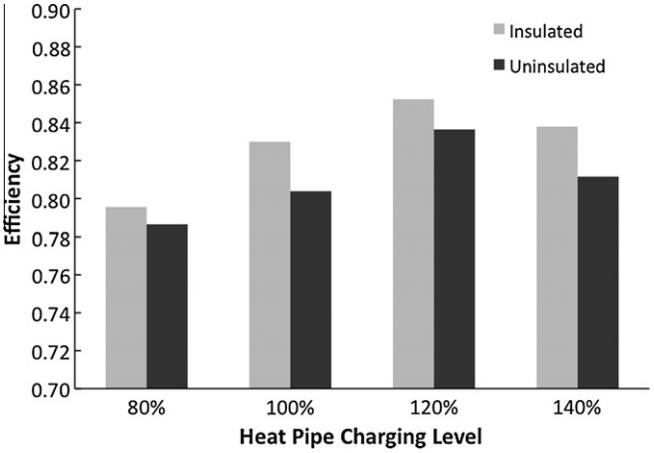

Fig. 13. Experimental overall system efficiency.

Parametric studies showed that a number of parameters had little effect on system performance relative to the baseline design, including number of covers, absorber thickness and material, collector edge insulation, heat pipe material, number of heat pipes, tank wall conductivity and thickness, tank to room conductance, condenser fins, and wall insulation. Compromises in these areas to reduce system cost while maintaining good thermal performance are possible. Parameters with greater effect on system performance were cover thickness and extinction coefficient, absorber surface properties and thermal storage capacity. Favored are a thin low-iron glass cover, a high-performance selective absorber surface and large storage capacity. As for other solar energy applications, load to collector ratio is an important parameter for sizing an economical system.

4.2. Experiments

Insulating the adiabatic section of the heat pipe improved efficiency for all fill levels, and a 120% fill level produced the highest efficiency. Adding fins to the condenser did not significantly improve system performance. System efficiency as high as 85% was demonstrated. Efficiency may be lower outdoors due to increased convective losses from wind and lower ambient temperature.

4.3. Matching of experiment and simulation

The conductance between the evaporator and condenser, K_{23}, was decreased substantially from 2311 to 150.2 W/m^2 K to achieve matching with the experiments. A potential reason is that the simulation includes no heat losses to the room between evaporator and condenser sections of the heat pipe, *i.e.*, that the adiabatic section is very well insulated. Imperfect insulation on the adiabatic section could account for part of the temperature difference between the

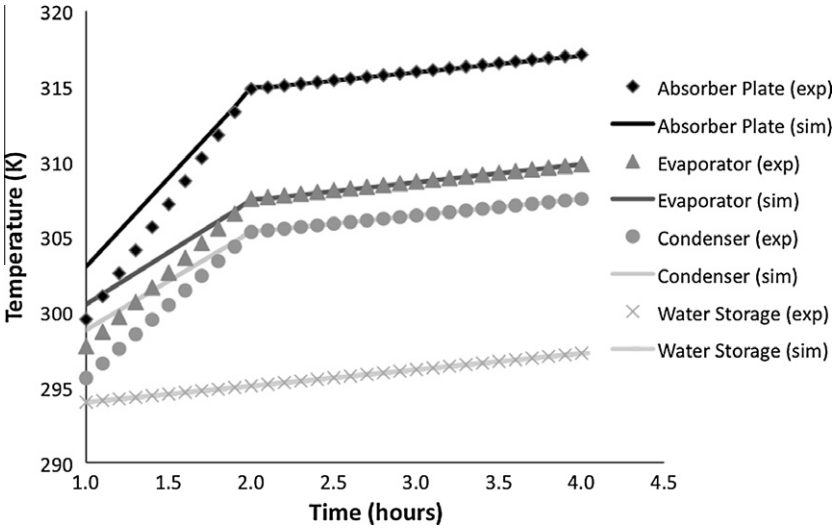

Fig. 14. Experimental (exp) and matched simulation (sim) predictions of temperature at various nodes in the prototype heat pipe wall.

Table 5
Thermal conductances before and after matching with experiment (W/m^2 K).

	K_{71}	K_{12}	K_{23}	K_{34}	K_{45}
Before matching					
Minimum	2.066	39.52	2311	22.21	385.2
Mean	2.204	39.52	2311	25.65	385.2
Maximum	2.416	39.52	2311	27.65	385.2
After matching					
Minimum	2.508	39.52	150.2	22.00	3.852E−07
Mean	2.672	39.52	150.2	25.15	3.852E−07
Maximum	2.921	39.52	150.2	27.38	3.852E−07

evaporator and condenser in the experimental data. Note that 150.2 W/m^2 K is still the highest conductance in the thermal network, thus nodal temperatures are relatively insensitive to this conductance, and it should not be unexpected that a large change would be required to achieve matching.

While there is a significant difference between the simulation and experimental data during startup due to the lack of nodal mass in the simulation, the temperatures matched well throughout the rest of the experiment.

5. Conclusions

The heat pipe system provided substantial gains in performance relative to conventional direct and indirect gain passive solar systems and, thus, presents a promising alternative for reducing building energy use.

Further modeling that includes both thermal and economic performance estimates is needed to develop a commercial unit. Economic performance depends on the climate and the load to collector ratio, as well as a number of factors related to the costs of the system and of conventional heating. For a simple example following the baseline case in Louisville (annual heating load of 2418 K days), a system producing a solar fraction of 50.6% on a building with load to collector ratio of 10 W/m^2 K offsetting \$0.10/kW h in conventional heating costs, simple payback would require a system cost of no more than \$29.36/m^2 per year, neglecting tax credits. A 2.5 m^2 unit (a reasonable size considering available glass widths and installation within a typical wall height), for instance, would pay back in ten years if its net cost were no more than \$734. As an example of the effect of the load to collector ratio, applying the system for a load to collector ratio of 100 W/m^2 K would provide a solar fraction of about 10% (see Fig. 9) and yield the same payback period for a system with net cost about twice as high.

Full-scale prototype tests in actual weather conditions are needed to validate system performance.

Acknowledgements

This work was conducted with the support of the Department of Energy (Grant DE-FG36-05GO85013) through the Kentucky Rural Energy Consortium, and with Department of Energy Grant DE-FC36-05GO85034.0.

References

Albanese, M.V., 2009. Development of an Integrated Solar Heat Pipe System for Improving Building Energy Efficiency. MEng Thesis, Department of Mechanical Engineering, University of Louisville, Louisville, KY.

Corliss, J.M., 1979. Evaluation of Heat Pipe Application for Passive Solar Systems, DOE Report, Department of Energy, Washington, DC.

Duffie, J.A., Beckman, W.A., 2006. Solar Engineering of Thermal Processes, third ed. John Wiley and Sons, New York.

Hay, J.E., Davies, J.A., 1980. Calculation of the solar radiation incident on an inclined surface, In: Hay, J.E., Won, T.K., (Eds.), Proceedings of the First Canadian Solar Radiation Data Workshop, Ministry of Supply and Services, Toronto, Canada, p. 59.

Incropera, F., DeWitt, D., 2002. Introduction to Heat Transfer, fifth ed. John Wiley and Sons, New York.

Klucher, T.M., 1979. Evaluating methods to predict insolation of tilted surfaces. Solar Energy 23 (2), 111–114.

Reindl, D.T., Beckman, W.A., Duffie, J.A., 1990. Evaluation of hourly tilted surface radiation models. Solar Energy 45 (1), 9–17.

Rice, W.J., 1984. Performance of passive and hybrid solar heating systems. International Journal of Ambient Energy 5 (4), 171–186.

Saatci, A.M., Olwi, R.R., 1989. Passive transport of solar energy downward by heat pipes. Energy 14 (7), 383–392.

Saman, W.Y., Abdulla, R.A. 1983. The US of heat pipes to reduce heat transmission through walls and roofs, solar world congress. In: Proceedings of the 8th Biennial Congress of the Int'l Solar Energy Society, pp. 380–384.

Susheela, N., Sharp, M.K., 2001. Heat pipe augmented passive solar system for heating of buildings. Journal of Energy Engineering 127 (1), 18–36.

URL 1, 2010. <http://eere.pnl.gov/building-technologies/index.stm> (accessed 05.25.10).

URL 2, 2010. <http://www1.eere.energy.gov/consumer/tips/home_energy.html> (accessed 05.25.10).

van Dijk, H.A.L., van Galen, E., Hensen, J., deWit, M., 1984. High performance passive solar heating system with heat pipe energy transfer and latent heat storage. Solar Energy R&D in the European Community, Series A: Solar Energy Applications to Dwellings 4, 118–130.

Varga, S., Oliveira, A.C., Afonso, C.F., 2002. Characterisation of thermal diode panels for use in the cooling season in buildings. Energy and Buildings 34, 227–235.